Received: 14 February 2023 | Revised: 30 March 2023 | Accepted: 11 April 2023

IET Renewable Power Generation

DOI: 10.1049/rpg2.12741

The Institution of Engineering and Technology WILEY

ORIGINAL RESEARCH

Numerical investigation on wake characteristics of floating offshore wind turbine under pitch motion

Rundong Tang[1] | **Renjing Cao**[1,2]

[1]Department of Mechanics and Aerospace Engineering, Southern University of Science and Technology, Shenzhen, China

[2]Guangdong Provincial Key Lab of Turbulence Research and Applications, Southern University of Science and Technology, Shenzhen, China

Correspondence
Renjing Cao, Department of Mechanics and Aerospace Engineering, Southern University of Science and Technology, Shenzhen 518055, China.
Email: caorj@sustech.edu.cn

Funding information
The Centers for Mechanical Engineering Education and Research at MIT and SUSTech (MechERE Centers at MIT and SUSTech).

Abstract

The floating offshore wind turbine platform is subject to six degrees-of-freedom motions due to the influence of wind, waves, and currents. To examine the impact of pitch motion on the wake characteristics of offshore wind turbines, this research focused on investigating the wind turbine wake under pitch motion using the RANS $k-\varepsilon$ model and the overset grid technique based on OpenFOAM. The simulation accounted for wind shear flow conditions and simplified the movements of the six degrees-of-freedom of floating platform. Results showed that the wind turbine wake recovery rate increased with pitch motion, and that the recovery rate increased with the frequency and amplitude of the pitch motion. The wind velocity recovery rate of near-wake was sensitive to small amplitudes, while the far-field wake was unaffected. When the amplitude was larger, pitch motion accelerated the wind velocity recovery rate in all wake areas, leading to more pronounced diffusion. These findings provide insight into the mechanism of wake generation and diffusion under pitch motion in floating offshore wind turbines and offer a basis for enhancing the wake deficit model of floating offshore wind farms.

1 | INTRODUCTION

Energy is crucial for the modern social and economic progress due to increasing demand. Wind energy, as a mature and promising renewable energy source, has garnered worldwide attention as a solution to the shortage of conventional energy and the deteriorating global environment. The utilization of wind energy in the global community gained momentum in the 20th century, with significant advancements in technology made from the mid-1980s to mid-1990s. Since then, wind power capacity has seen a rapid average annual growth of 30%, making it one of the fastest-growing energy sources globally [1]. Wind turbines, being a modern, secure, and clean energy source, have gained widespread recognition and large-scale development in countries with abundant wind resources.

The floating offshore wind turbine (FOWT) consists of an impeller, a floating platform, and a mooring structure. The idea of an FOWT was first introduced by Heronemus in 1972 [2], who installed a series of miniature wind turbines on a floating platform, which serves as the prototype for the present-day FOWT. FOWTs have been gaining increasing attention in the wind energy sector since the 1980s, especially with the advancement of offshore wind power in Europe. Compared to conventional onshore stationary wind turbines, FOWTs have received greater attention in recent years. They are mainly used in far-sea areas over 200 m from shore with water depths greater than 50 m [3]. Unlike fixed offshore wind turbines, FOWTs can be installed in deep-water areas with abundant wind resources and harsh offshore climate conditions, making them more economically viable [4]. The movements of the wind, waves, and currents cause the FOWT platform to move in the direction of six degrees-of-freedom (6-DOF), which can greatly impact the aerodynamic performance and wake characteristics of wind turbine [5]. Among these movements, the pitch motion has a significant influence on the performance of the wind turbine as it changes the pitch state in line with the incoming wind velocity. The operating environment of the floating wind turbines at sea is also complex, with wind shear and atmospheric turbulence affecting floating wind turbines. The wake of the wind turbine can have a dynamic effect on the blades, affecting the wake, aerodynamic performance, and structural response of offshore wind turbines. The diffusion and development of the wake of the FOWT is different from that of onshore wind turbines due to the friction between the wake and the moving boundary of

sea waves. Actuator disk models and actuator line models, commonly used in engineering, struggle to reveal the wake diffusion and development processes of wind turbines in complex offshore conditions. Hence, this study simulated the pitch motion of the FOWT and analyzed its wake characteristics.

The study of FOWTs has seen a significant amount of research by various scholars, using diverse methods and approaches. In 2009, Jonkman et al. [6] from the National Renewable Energy Laboratory (NREL) developed an FAST model for the tension-leg platform, spar buoy and barge, using NREL 5 MW wind turbine as a basis, establishing a foundation for FOWT studies. This work laid the foundation for the study of floating wind turbines. Jonkman and his team [7] later utilized the BEM method for dynamic calculations of floating wind turbines and evaluated the advantages and disadvantages of different model methods. Nianxin Ren et al. [8], based on the 5-MW offshore wind turbine model developed by NREL, proposed two coupling models of the tension-leg floating platform and mooring system and performed separate time-domain analysis of wind loads and hydrodynamic coupling. Wei et al. [9] proposed a method for analyzing the bearing capacity of FOWT support structures using incremental wind wave analysis (IWWA) and demonstrated this method with an example calculation of a single-pile floating wind turbine and a sheathed floating wind turbine in the Atlantic Ocean.

Furthermore, several scholars have attempted to optimize and improve numerical models for FOWTs through various computational methods. In 2006, Zambrano et al. [10] used the Newton Rung-Kutta method to analyze the 6-DOF of a mooring floating platform equipped with three wind turbines and simulated the longitudinal, vertical, and transverse motions of the platform. Micallef and his colleagues [11] performed numerical simulations on a NREL 5 MW wind turbine during surge motion by using Navier–Stokes models based on the actuator disk models, BEM method, and a generalized dynamic wake model. Tran and Kim [12] studied the effect of the vortex-wake-blade interaction, caused by the periodic pitch motion of the impeller, on the aerodynamic performance of the FOWT using unsteady computational fluid dynamics. Lei et al. [13] analyzed the floating wind turbine through a multi-body dynamics model, simplifying the non-linear dynamic coupling between the mooring system forces and the structural motion, and compared it to the offshore stationary wind turbine. Chen [14] conducted unsteady numerical simulations of the floating wind turbine under given sea conditions using the unsteady RANS method and compared the results of BEM method and vortex method to examine the motion response. ArcVera Renewables, a renewable energy project technical services provider, used a high-fidelity weather prediction model in wind farm parametrization software to study the far-field wake deficit of wind turbines and found that the impact of high-power offshore wind turbine wake could reach as far as 100 km, concluding that common engineering models significantly underestimate the wind energy deficit caused by far-field wake [15].

In addition to numerical simulations, some researchers have verified their model results through experimental studies. Bjørn Hanson et al. [16] compared their experimental findings from the 1:47 scale model of HYWIND floating offshore turbine with the simulation results from HAWC2 models of Risø National Laboratory and SIMO/RIFLEX models of MARINTEK. The study made use of active damping control to avoid resonance between the tower and impeller, which was successfully validated through the experiment. Hand et al. [[17] from NREL examined the aerodynamic load of the turbine impeller at a fixed yaw angle, analyzed the effect of highly dynamic wind loads, and verified that three-dimensional effects are prevalent in actual wind turbine operation. Murfet and Abdussamie [18] explored the load and dynamic response of a floating platform under the influence of wind and waves coupling by using the TLPWT model based on NREL 5MW wind turbine. Wang et al. [19] compared the accuracy of domestic and foreign wind velocity and power prediction models, analyzing their physical, statistical, and hybrid approaches across different time scales. According to Wang, evaluating the performance of various models is challenging due to differing modelling assumptions and ideas. However, despite their limitations, although their predictive models are not ideal for wind turbine wake prediction under all conditions, these models remain the most cost-effective and practical power forecasting tools, enhancing the reliability of wind power generation in wind farms.

According to the above literature review, there have been numerous articles on wake characteristics for floating wind turbines. However, research on the numerical simulation of the wake of pitching motion wind turbines based on the OpenFOAM has not been widely explored. Under different frequencies, floating wind turbines will experience stronger impacts and wear, which will affect their power output. Therefore, the speed, acceleration, and motion range of wind turbines themselves are relatively large, and wind turbines will have different aerodynamic responses and wake characteristics. This study aims to uncover the effects of wake characteristics, diffusion mechanisms, and unsteady aerodynamic forces on the wake of a single NREL 5 MW wind turbine under pitch motion through simulation. The simulation calculation uses the $k-\varepsilon$ model based on OpenFOAM, establishes a wind field model, sets wind shear flow and atmospheric turbulence conditions, simplifies the 6-DOF movement of the floating platform with the simple harmonic pitch motion equation, and establishes the dynamic mesh. The findings of this study provide a more accurate physical basis for evaluating the wind resources of offshore wind farms.

2 | NUMERICAL METHODS AND FOWT MODEL

The numerical simulations are based on the non-stationary, three-dimensional, incompressible Navier–Stokes equations:

$$\begin{cases} \nabla \cdot u = 0 \\ \dfrac{\partial u}{\partial t} + (u \cdot \nabla) u = -\dfrac{1}{\rho}\nabla p + \nu \nabla^2 u \end{cases} \tag{1}$$

TABLE 1 The parameters of 5-MW wind turbine

Properties	Value
Rating	5 MW
Rotor orientation, configuration	Upwind, 3 Blades
Rotor diameter	126 m
Hub height	90 m
Cut-in, rated, cut-out wind speed	3 m/s, 11.4 m/s, 25 m/s
Cut-in, rated rotor speed	6.9 rpm, 12.1 rpm
Rated tip speed	80 m/s
Rotor mass	110,000 kg

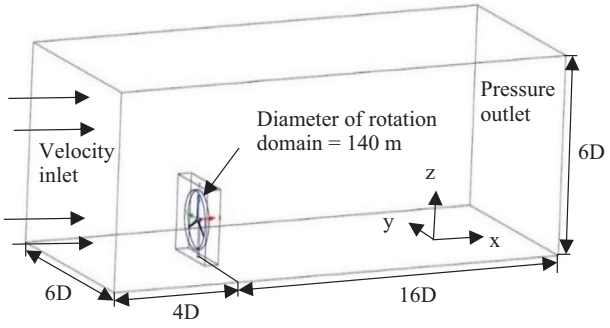

FIGURE 1 Schematic diagram of computational domain.

Here u is fluid velocity, t is time, ρ is air density, p is pressure, and ν is kinematic viscosity coefficient.

In this study, the pitch motion of the NREL 5 MW wind turbine was simulated utilizing the RANS $k-\varepsilon$ turbulence model and an overlapping mesh and dynamic grid technique. The flow field was resolved by using the OverPimpleDyMFoam solver of OpenFOAM, which has a well-established reputation for its efficiency and precision in tackling intricate flow scenarios. This solver is widely used by researchers and engineers in academia and industry alike, due to its proven ability to effectively simulate wind turbines. The discrete equations were discretized using a second-order upwind scheme, further ensuring the accuracy of the simulation results. The time step was selected based on the courant number between 0.01 and 0.1 s, and the calculation time required for a simulation was approximately 1 month. The computational device was the 'Taiyi' supercomputer cluster at the Center for Scientific and Engineering Computing.

2.1 | Numerical model

The numerical simulation was performed on the NREL 5 MW wind turbine and the specific parameters were sourced from an article by Jonkman [20]. The wind turbine features a diameter of 126 m, a rated inlet wind velocity of 11.4 m/s, and a rated velocity of the impeller at 12.1 rmp. These parameters serve as a basis for the simulation and allow for the accurate representation of the wind turbine and its performance. Through the simulation process, important information was revealed regarding the power and wake characteristics of the NREL 5 MW wind turbine, providing valuable information into the study (Table 1).

2.2 | Computational domain

The computational domain of the simulation included the flow field, pitch field, and rotation field, with the pitch and rotation fields overlapping mesh regions. The height and the width of the cuboidal flow field were both set as $6D$ (D is the diameter of the impeller). The x-axis was designated as the direction of the velocity flow, the y-axis was the horizontal direction, and the z-axis was the vertical direction. The wind turbine impeller was located at the centre of the computational domain, $4D$ away from the velocity inlet surface. To ensure adequate diffusion of the wind turbine wake, the outlet surface was placed $16D$ away from the impeller. The rotational domain was represented as a cylinder with a diameter of 140 m and a height of 12 m, while the pitch domain was represented as a cuboid with dimensions of $0.5\ D \times 1.5\ D \times 1.5\ D$. A schematic diagram of the computational domain is shown in Figure 1.

2.3 | Boundary conditions

The inlet of the flow field was defined as a velocity inlet boundary, while the outlet was defined as a pressure outlet. The bottom wall, blade surface, tower surface, and hub surface were all set as non-slip boundaries, while the upper wall was defined as a slip boundary and the two sides were symmetric boundary conditions. The wind shear formula was applied to better model the marine atmospheric environment. The inlet velocity of the simulation was set using a user-defined function (UDF) to display an exponential distribution along the z-axis, creating a shear-inlet condition. This approach improved the accuracy of the simulation, allowing for a more realistic representation of the marine atmospheric conditions and its effect on the model being studied. The formula of wind velocity profile is as follows [21]:

$$v(h) = v_0\left(\frac{h}{H}\right)^a \tag{2}$$

Here $v(h)$ is the wind velocity at the height h from the ground, v_0 is the wind velocity at the height of the hub, and the value is the rated wind velocity of the wind turbine. $H = 90$ m is the height of the hub, $a = 0.1$ is the wind velocity profile index. According to a reference [22], the turbulence strength has an impact on the wind turbine torque; therefore, a turbulence level of 5% is applied to the incoming flow during the calculation to account for this effect (Figure 2).

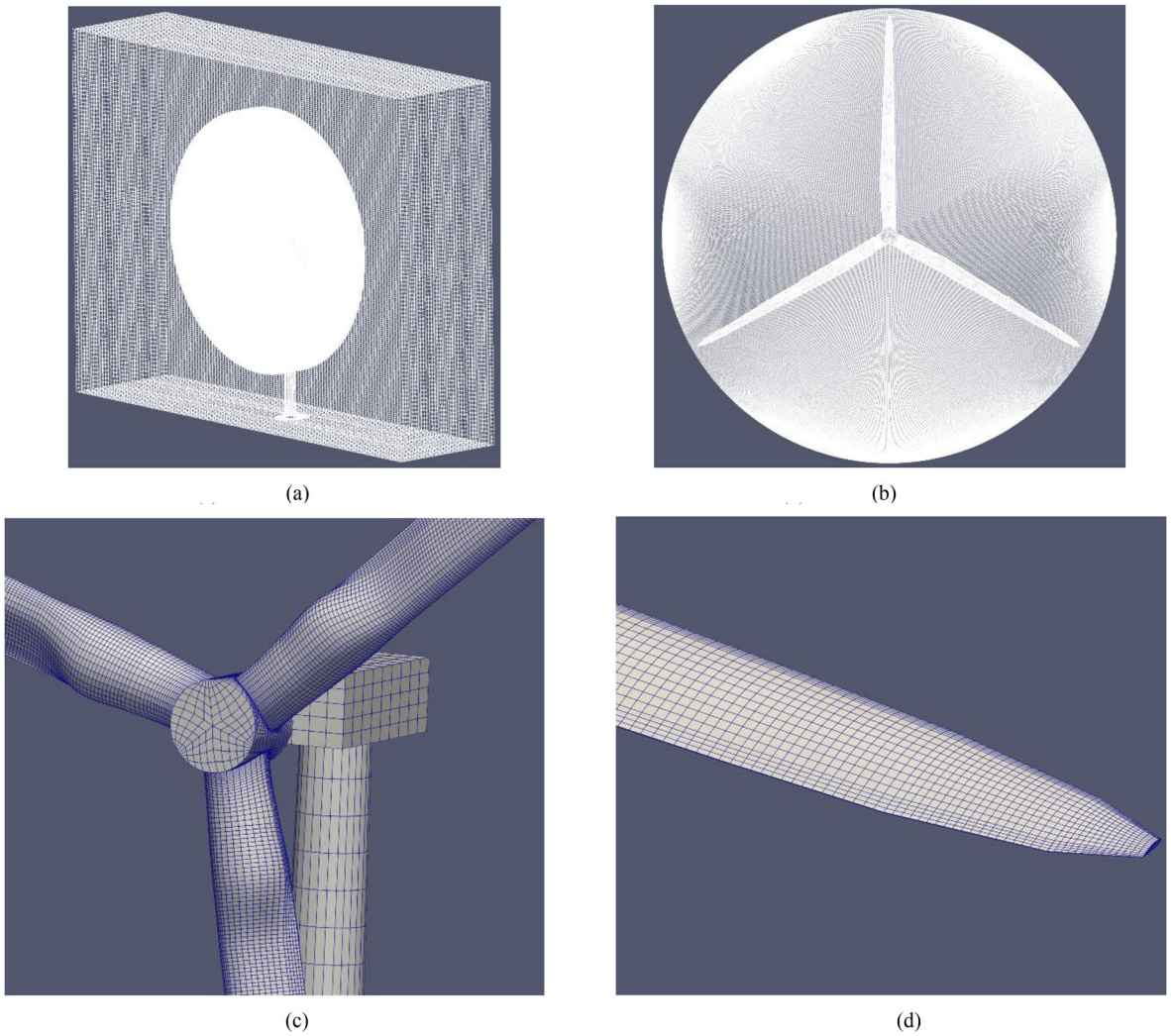

FIGURE 2 Grids of computational domain. (a) Pitch domain mesh. (b) Rotation domain mesh. (c) Blade root surface mesh. (d) Blade tip surface mesh.

2.4 | Computational mesh and mesh independence

The pre-processing software ICEM was utilized to construct the structural grid of the computational model. To ensure the accuracy of the calculations for the aerodynamic properties of the blades, mesh refinement was applied to the O-blocks in the blade regions. The mesh of the flow domain was constructed using sparse grids, and additional refinement was applied to the mesh of the pitch domain and its surrounding area.

In order to accurately simulate the pitch motion of the wind turbine, this study designed four computational domains with varying grid numbers. The grid numbers were 7.04 million, 8.65 million, 14.45 million, and 20.23 million, as demonstrated in Table 2. The numerical results were compared to the torque values at the rated wind velocity, as specified in reference [23]. The results showed that the computational domain with 14.45 million grids was an appropriate compromise between accuracy and computational efficiency. While using a higher number of grids would result in increased accuracy, the computational time would also significantly increase. Conversely, using fewer grids would lead to faster convergence, but at the cost of insufficient accuracy. Taking these factors into consideration, this study opted to use the computational domain with 14.45 million grids, with the smallest mesh size being 0.01 m. This high level of mesh refinement was necessary to ensure the precision and accuracy of the simulation results.

2.5 | Pitch motion conditions

The overlapping mesh technology of OpenFOAM facilitated the simulation of the relative motion of the wind turbine by dividing the computational region into three components: flow field, pitch field, and rotation field. The pitch field and rotation field mesh were designed to remain relatively stationary while

TABLE 2 Wind turbine torque of different cells numbers

Cells number (10^4)	704	865	1445	2023	Designed value
Torque (N·m)	3.72×10^6	3.81×10^6	3.93×10^6	3.96×10^6	4.08×10^6
Errors	8.8%	6.6%	3.7%	2.9%	

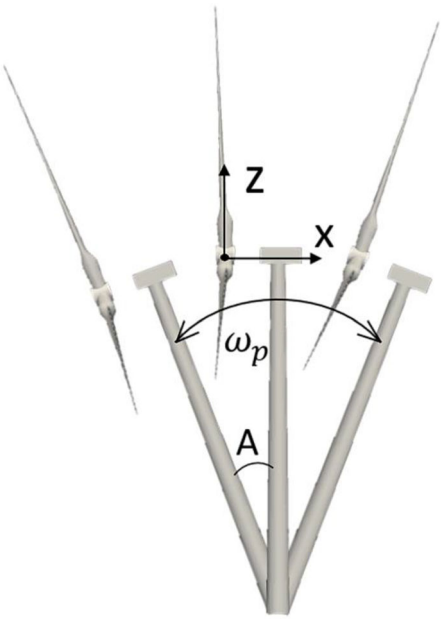

FIGURE 3 Schematic diagram of pitch motion.

oscillating at the same frequency and amplitude. The angular variations of the pitch motion were accurately modelled through the compilation of UDF code, which was based on the angular velocity formula, thereby allowing for a precise simulation of the pitch motion of the wind turbine. The formula of the pitch motion is given by [14]

$$\omega_p = 2\pi f A_p \cos(2\pi ft) \tag{3}$$

Here A_p represents the amplitude of pitching, ω_p represents the angular velocity change of pitching motion, and f represents the motion frequency. The rotational domain rotates around the x-axis through the centre of the rotational domain at a rated speed of 12.1 rpm (Figure 3).

To simulate the pitch motion of a wind turbine, the design in references [14, 24] was considered and its effects on rated wind velocity and regular waves on floating wind turbines were taken into account. By changing pitch frequency and amplitude, the pitch motion of varying intensities was simulated. Four combinations of two groups of amplitude ($A = 1°$, $A = 4°$) and two groups of frequency ($f = 0.1$ Hz, $f = 0.2$ Hz) were selected for numerical calculation, along with a normal case (no pitch motion), resulting in a total of five cases. The computational parameter settings for each of the cases are presented in Table 3.

TABLE 3 Pitch motion cases

Case	Rotor speed n (rpm)	Amplitude A (°)	Frequency f (Hz)
1	12.1	0	0
2	12.1	1	0.1
3	12.1	1	0.2
4	12.1	4	0.1
5	12.1	4	0.2

3 | RESULTS AND DISCUSSION

3.1 | Power analysis of wind turbine

Power analysis of wind turbine is a crucial aspect in the design, operation, and maintenance of wind energy systems. The primary objective of power analysis is to determine the amount of electrical power that a wind turbine can generate under specific wind conditions, such as wind velocity and direction. This information is used to optimize the turbine design for maximum power, and to ensure that the turbine is operating efficiently and safely [25]. The results of power analysis are used to evaluate the viability of a wind energy project, and to support decision-making around the design, operation, and maintenance of wind turbines.

3.1.1 | Power of wind turbine without pitch motion

The power of the NREL 5 MW wind turbine was analyzed in the absence of experimental data. To fill this gap, the power curve calculated by Jonkman [20] using the FAST software in 2009 was referred to and is presented in Figure 4. The accuracy of the numerical model was confirmed by comparing the results from OpenFOAM simulations with the power curve obtained from FAST, under different incoming flow velocities. Table 4 provides a clear illustration of the relationship between the incoming flow velocity and steady rotor speed of the wind turbine, which was taken from the reference [26]. The comparison between the results from OpenFOAM and FAST provides valuable validation of the power of the NREL 5 MW wind turbine modelled using OpenFOAM and its performance under varying wind conditions.

In the analysis of the performance of the wind turbine, Figures 4 and 5 provide insights into the calculated power

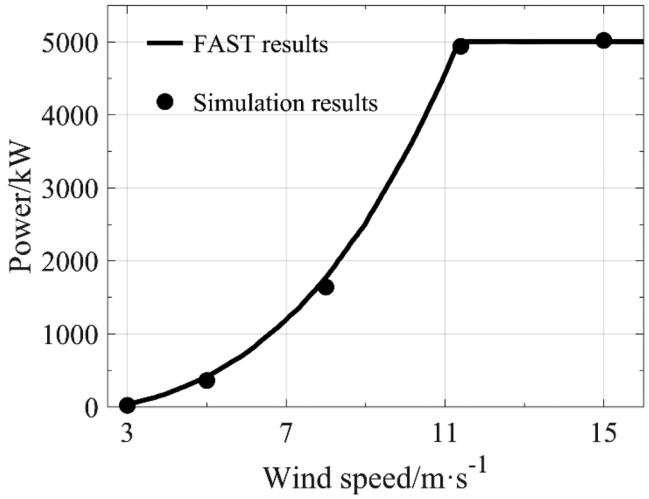

FIGURE 4 Comparison of FAST power curve with OpenFOAM results.

TABLE 4 Results of wind turbine power under different wind velocities

Incoming flow velocity (m/s)	Rotor speed (rpm)	Power (MW)
3	6.9	0.02
5	6.9	0.36
8	9.7	1.67
11.4	12.1	4.94
15	12.1	5.02

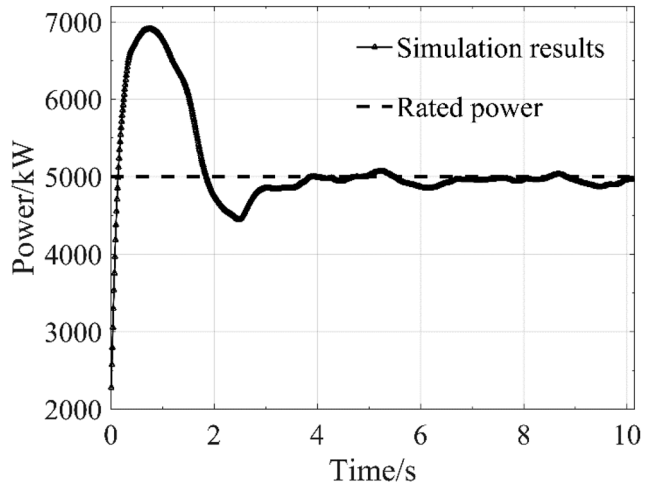

FIGURE 5 Power curve of wind turbine with time.

as determined by OpenFOAM and FAST. Figure 4 illustrates that, in general, the calculated power results from OpenFOAM and FAST are similar, with no significant differences observed. However, it should be noted that when the incoming wind velocity does not exceed the rated wind velocity, the calculated power determined by OpenFOAM is slightly lower than that obtained from FAST. This discrepancy can be attributed to the fact that the simulation model utilized in this study, which was based on OpenFOAM, did not consider the initial elevation angle of the impeller in its calculations. As a result, the calculation of power was reduced, which led to the observed difference in results between the two methods. Figure 5 presents the power curve of NREL 5 MW wind turbine for Case 1 over a time span of two periods of rotation. Over the course of these two periods, the power generated by the wind turbine gradually stabilized at the rated power level, demonstrating the stability and reliability of the system under steady-state conditions. The results show that the wind turbine performs consistently and reliably under steady-state conditions.

3.1.2 | Power of wind turbine under pitch motion

Figure 6 shows the results of the power of a wind turbine based on OpenFOAM at different pitch frequencies and amplitudes. The analysis was performed in comparison to other unsteady models such as the UBEM models and unsteady CFD models [12]. The results show that even under conditions of small pitch frequencies and amplitudes, the aerodynamic power of the wind turbine exhibits significant fluctuations. The fluctuations in the power of wind turbine are magnified as the frequency and amplitude of the pitch increase, with the pitch motions resembling general harmonic motions. In cases 3 and 5, which involved larger pitch frequencies, the power fluctuation curve first slows down and then accelerates during the intermediate stages, due to the three-dimensional effects of the model. The results from OpenFOAM suggest that the peak values are larger than those from the unsteady CFD model for slight pitch motion and similar to those from the UBEM models for strong pitch motion. However, the more realistic three-dimensional effects of the unsteady CFD model in the simulations result in more drastic power fluctuations, with peak values being larger than those from the UBEM models. The results indicate that the performance of wind turbine is greatly influenced by the pitch frequency and amplitude, with larger frequencies and amplitudes leading to greater fluctuations in the power output.

The results of four cases of the power calculated using OpenFOAM under different pitch frequencies and amplitudes are presented in Figures 7a and 7b. As shown in Figure 7a, the results indicate that even under conditions of small pitch frequencies and amplitudes, the aerodynamic power of the wind turbine exhibits significant fluctuations. These fluctuations are magnified as the frequency and amplitude of the pitch increase, with the pitch motions resembling general harmonic motions. In Figure 7b, a comparison of the minimum, average, and maximum wind turbine power for the four pitch motions is presented. Figure 8 shows the positions corresponding to the peak state and the bottom state of the power curves of the wind turbine in different cases. The results suggest that as the wind turbine moves upwind towards the equilibrium position in the pitch motion, the attack angle of the blades and the relative wind velocity increase, leading to an increase in instantaneous power.

According to the BEM method, the torque of the wind turbine is proportional to the cubic power of the velocity [27]. As the frequency of the pitch motion changes, the induced veloc-

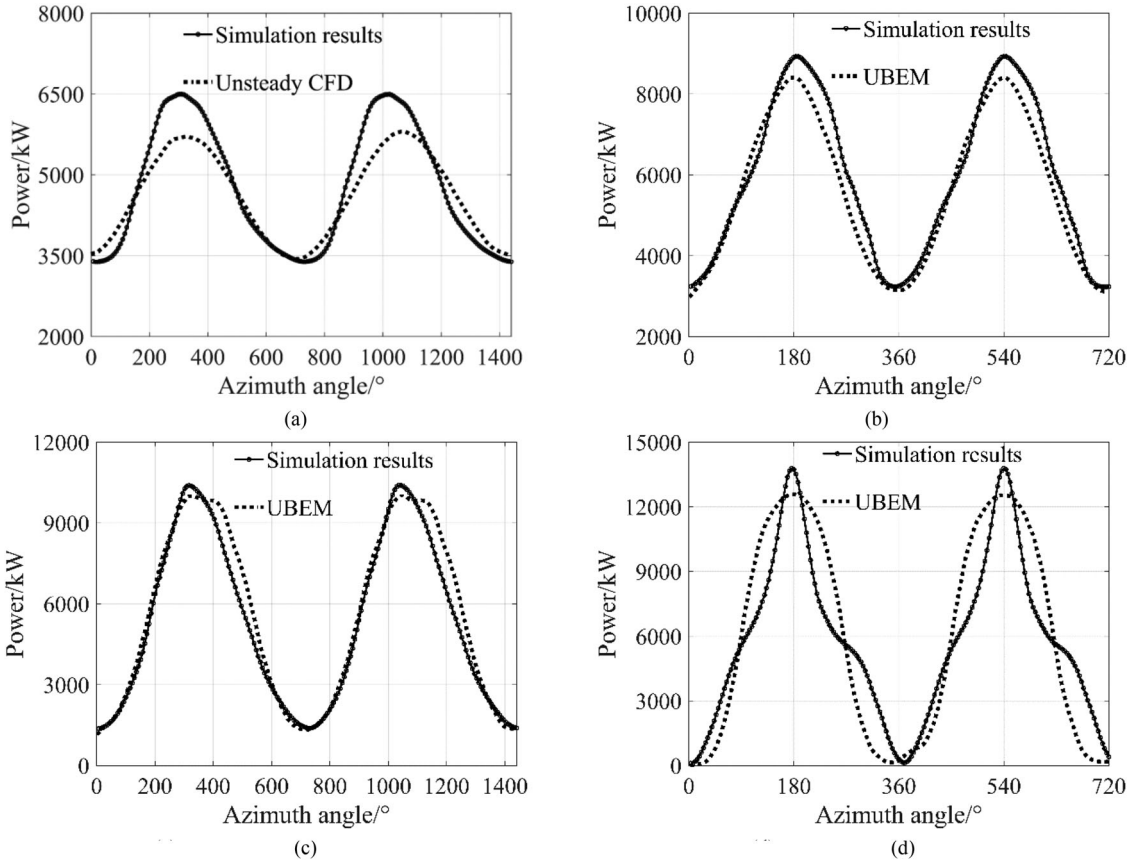

FIGURE 6 Comparison of OpenFOAM power results with other unsteady models under pitch motion. (a) Case 2, $A = 1$ m, $f = 0.1$ Hz. (b) Case 3, $A = 1$ m, $f = 0.2$ Hz. (c) Case 4, $A = 4$ m, $f = 0.1$ Hz. (d) Case 5, $A = 4$ m, $f = 0.2$ Hz.

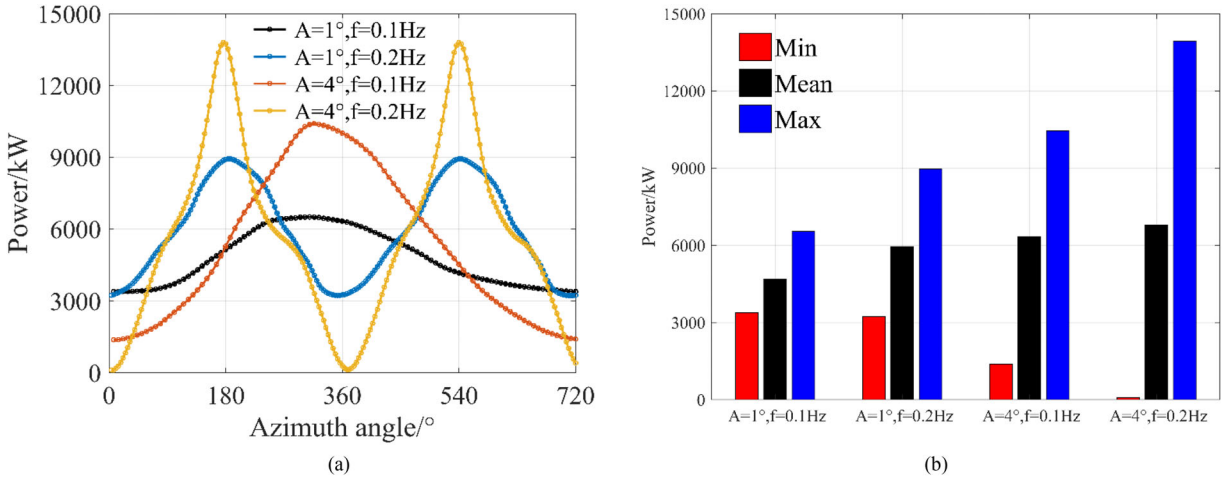

FIGURE 7 Comparison of the OpenFOAM power results under pitch motion. (a) Total power curves of pitch motion. (b) Extreme and average power of pitch motion.

ity changes, resulting in significant changes in the torque. The swept area of the wind turbine remains constant during the pitch motion of the platform. As the frequency and amplitude of the pitch motion increase, the average instantaneous power of the wind turbine also increases, resulting in larger peak and smaller bottom values. Moreover, high-frequency pitch motions produce more power fluctuation periods, significantly affecting the power of the wind turbine. For example, when the pitch frequency and amplitude are small, such as $A = 1°$ and $f = 0.1$ Hz, the maximum power of the wind turbine is 6.5 MW, with a minimum power of 3.39 MW. However, when the pitch motion is more intense, such as $A = 4°$ and $f = 0.2$ Hz, the peak power

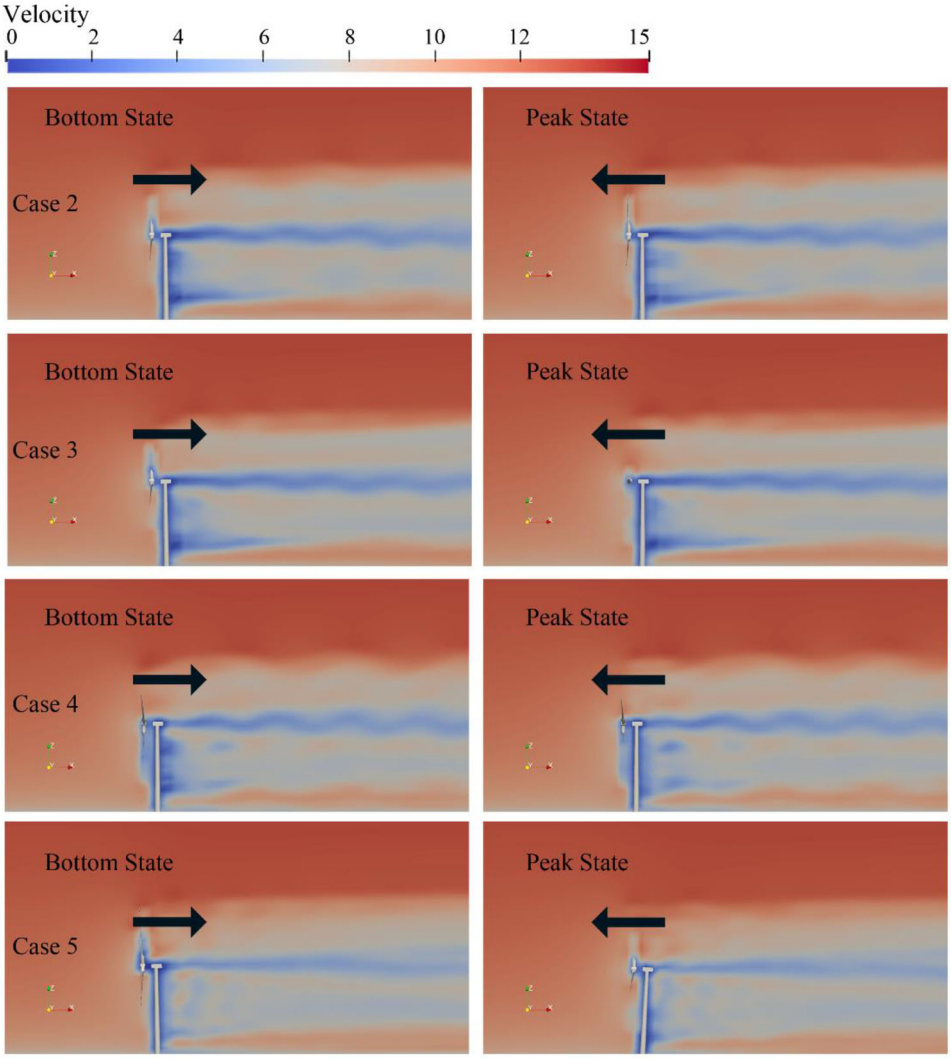

FIGURE 8 The wind turbine positions corresponding to minimum/maximum power under pitch motions.

can reach 13.79 MW, approximately three times the rated power, with the bottom value close to 0. The analysis illustrates the impact of pitch frequency and amplitude on the performance of the wind turbine, with larger frequencies and amplitudes resulting in pronounced fluctuations in the power. Such fluctuations will dramatically increase the additional fatigue load on the blades of the wind turbine and cause significant degradation of the service life.

3.2 | Wake analysis of wind turbine

The results of the simulation of the wind turbine wake, computed using OpenFOAM, were found to be in good agreement with actual measurements. The circumferentially averaged method was employed to process the results and obtain the mean velocity distribution curves in the wake area for case 1. As depicted in Figure 9, these curves were compared to the wind velocity profile in the wake area, which was measured using unmanned aerial vehicle (UAV) data in a coastal wind farm [28]. UAV wind measurement represents a recently developed method that has the potential to enhance the efficiency of traditional wind measurement techniques. Li proposed a UAV-based approach for measuring the wake characteristics of wind turbines and compared the measured wind velocity of the UAV in the experiment to the predicted wind velocity. The comparison, shown in Figure 9, demonstrates that the wake velocity distribution curves obtained from the OpenFOAM simulation are in alignment with those measured by the UAV in the experimental site. Furthermore, the simulated wake recovery situation is also consistent with the actual scenario. These findings provide evidence of the accuracy and reliability of the OpenFOAM simulation in predicting the wake characteristics of wind turbines.

The actuated line model is a widely used tool in the numerical calculation of wind turbines, particularly in engineering applications, due to its simple calculation procedure, quick processing time, and acceptable accuracy for specific conditions. Despite

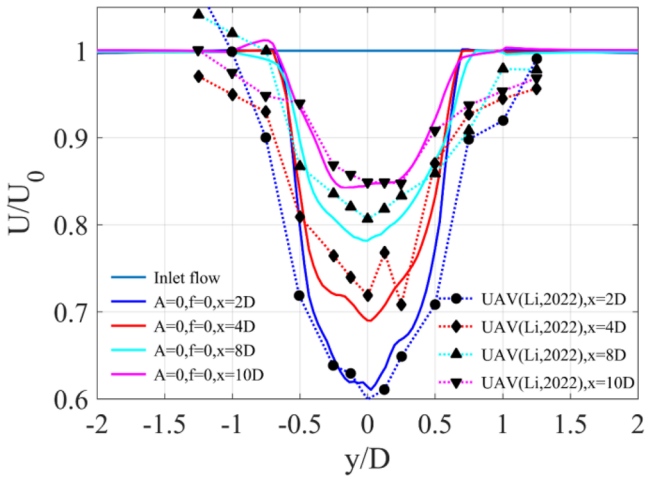

FIGURE 9 Comparison of mean velocity distribution of wind turbine wake with UAV measured results.

its widespread usage, the actuated line model falls short in capturing the intricacies of non-stationary flows and does not account for 3D effects in its numerical calculations. This study resorted to the 3D wake model of the Sun [29], and compared the mean wake velocity distribution curve obtained using OpenFOAM with that calculated using the actuated line model. Figures 10a and 10b show the velocity distribution of the wind turbine wake through the centre of the impeller in the horizontal and vertical directions, respectively, under the condition of shear flow without pitch motion. The results were extracted from the wind velocity distributions in the downstream planes at distances of 3D, 5D, 7D, 9D, and 15D from the impeller centre. The results indicated that the incoming flow velocity was significantly reduced in the wake flow field, with the greatest deficit of wind velocity observed in the region directly behind the nacelle. The maximum wind velocity deficit in the $x = 3D$ downstream region was estimated to reach 35% of the incoming flow velocity. As the wake progressed downstream, it underwent momentum exchange with the flow outside the wake flow field, leading to a gradual recovery of the wake wind velocity. The wake wind velocity was found to have recovered to 90% of the normal incoming flow velocity at $x = 15D$ downstream. The actuated line method, on the other hand, overestimated the recovery rate of the wake velocity and the expansion angle of the wake. Additionally, the actuated line method failed to account for the tower shadow effect generated by the wind turbine nacelle and tower, which resulted in an underestimation of the wake velocity deficit.

The velocity deficit distribution curves of the wake are depicted in Figures 11 and 12, which display a comparison of the wake wind velocity distribution between the cases under pitch motion and the case 1. In comparison to the baseline scenario, the pitch motion of cases 2–5 has a noticeable impact on the flow field near the impeller, resulting in an increase of turbulence levels in the near-field wake region and subsequently expediting the wake recovery rate.

The data depicted in Figures 11 and 12 highlights that the effect of pitch motion on the wake velocity in the near-field wake area is significant and serves to expedite the process of wake recovery. It was observed that as the frequency and amplitude of the pitch motion increased, the recovery rate of the wake was further accelerated. In contrast, the results show that slight pitch motion has a limited effect on the wake recovery in the far-field wake region. However, when the pitch amplitude was 4° and the frequency was 0.2 Hz, a marked improvement in the recovery rate of the far-field wake was observed. In cases 2 and 4, when the amplitude was 1°, the wake velocity at $x = 15D$ downstream in the wake region was consistent with that of case 1. In contrast, in cases 3 and 5, with an amplitude of 4°, the wake velocity at $x = 15D$ downstream recovered faster, with velocities that were closer to the inflow velocity. It should be noted that the results obtained from this study suggest that the pitch motion has a significant impact on the wake velocity distribution, particularly in the near-field wake region. The findings provide important insights into the wake characteristics of wind turbines and can inform the design and optimization of wind turbines to enhance their performance and efficiency. Further research is needed to fully understand the impact of pitch motion on the wake velocity distribution, and to determine the optimal conditions for wake recovery in wind turbines.

The velocity contours and vertical cross-sectional views of the wind turbine wake are depicted in Figures 13 and 14. Figure 13 presents a cross-sectional view of the centre of the wind turbine through the vertical x–z plane at $y = 0$, while Figure 14 displays the velocity contours on the vertical y–z cross section plane at various downstream distances ($x = 3D$, $5D$, $7D$, $9D$, and $15D$). As observed in Figure 13, the wake diameter is slightly larger than the impeller diameter, with a smaller wake expansion angle and the area of the largest velocity deficit being the wake centre area directly behind the nacelle. For cases where the frequency and amplitude of pitch motion are small, the velocity contours of the wake flow field are found to be consistent with those in the reference case 1. As the pitch amplitude and frequency increase, the wind rotational field becomes compressed and a prominent interface of periodic fluctuations appears between the edge of the near-field wake area and the wake centre. This results in faster mixing of the wake centre directly behind the nacelle with the surrounding wake flow, leading to an acceleration in the wind velocity recovery in the wake region. The far-field wake, which previously had an obvious centre, gradually begins to dissipate. The recovery rate of the far-field wake is particularly improved when the pitch amplitude is 4° and the frequency is 0.2 Hz.

Figure 14 demonstrates that the wake flow in the five cases spreads to varying degrees and gradually mixes with the fluid outside the wake region as the downstream distance increases. The violent squeezing of the wake area by the impeller under the condition of high pitch amplitude (4°) in cases 3 and 5 accelerates the recovery of the wake velocity. The far-field wake in these cases is found to exhibit more pronounced diffusive phenomena compared to the cases with small amplitude. At $x = 15D$, the wake velocity is consistent with the incoming flow

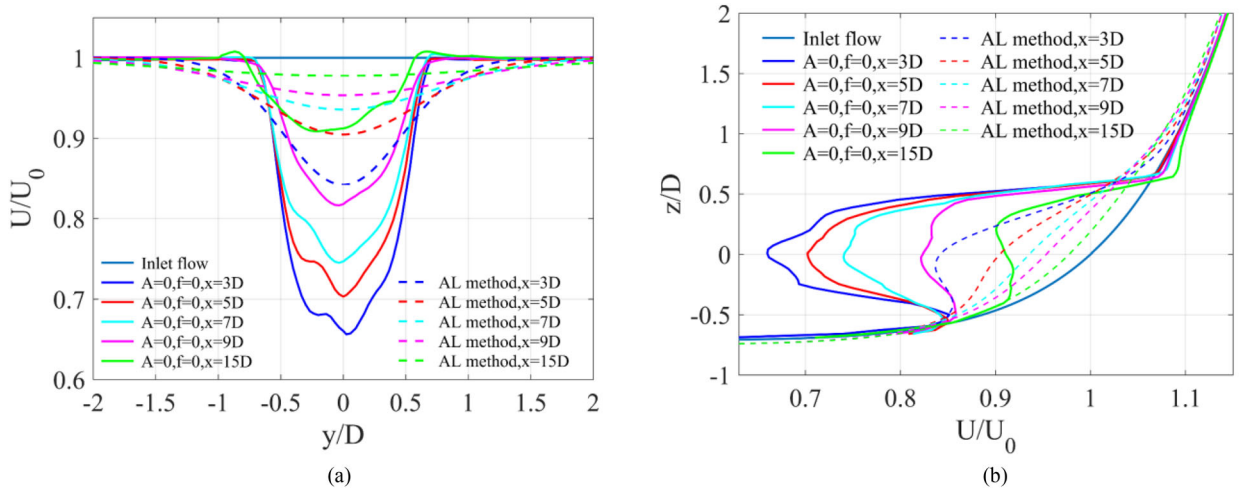

FIGURE 10 Comparison of mean velocity distribution of wind turbine wake with actuator line method results. (a) Case 1 ($A = 0, f = 0$) horizontal wind velocity distribution curves. (b) Case 1 ($A = 0, f = 0$) vertical wind velocity distribution curves.

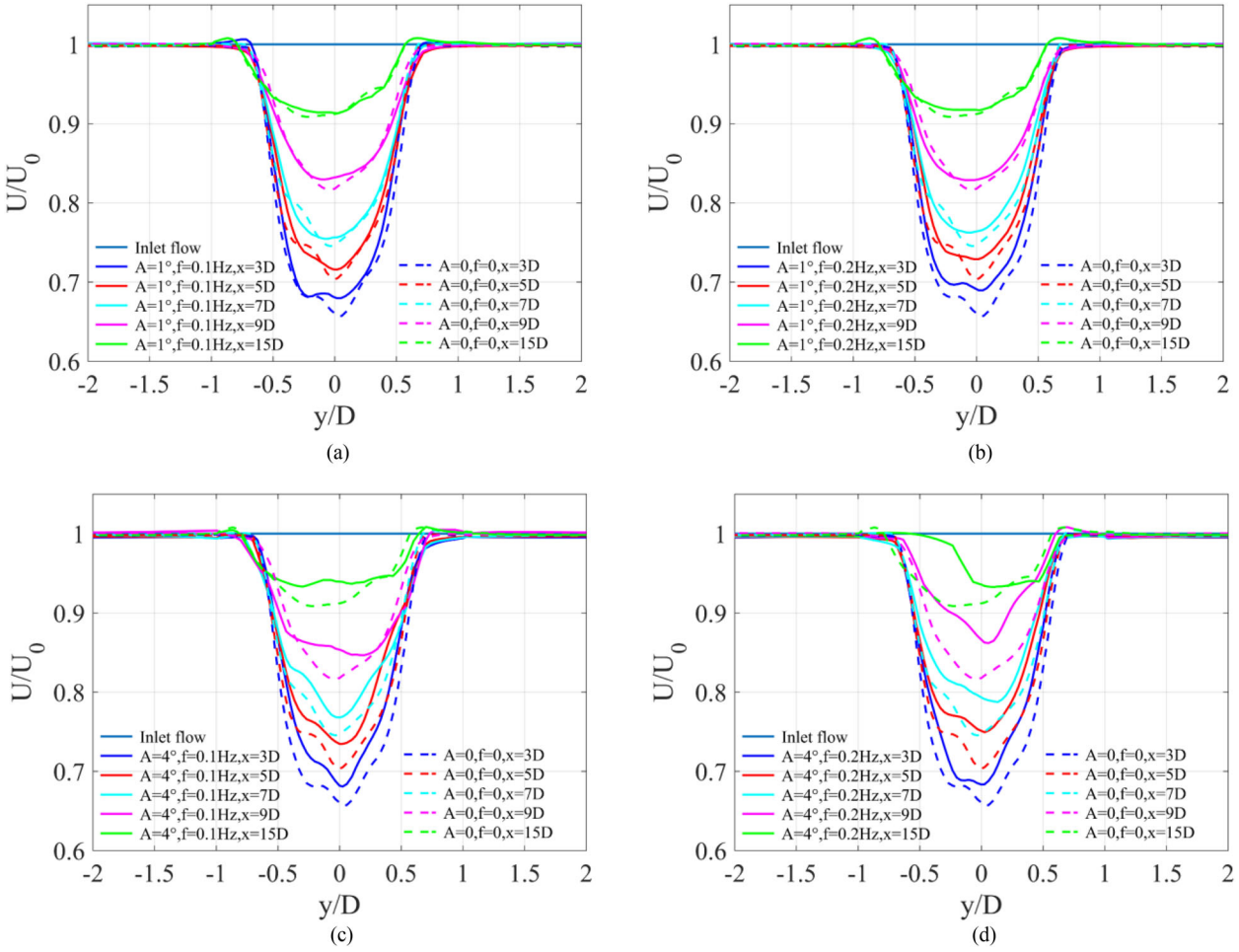

FIGURE 11 Comparison of the horizontal mean velocity distribution curve of wake under pitch motion with the results without pitch motion. (a) Case 2, $A = 1$ m, $f = 0.1$ Hz. (b) Case 3, $A = 1$ m, $f = 0.2$ Hz. (c) Case 4, $A = 4$ m, $f = 0.1$ Hz. (d) Case 5, $A = 4$ m, $f = 0.2$ Hz.

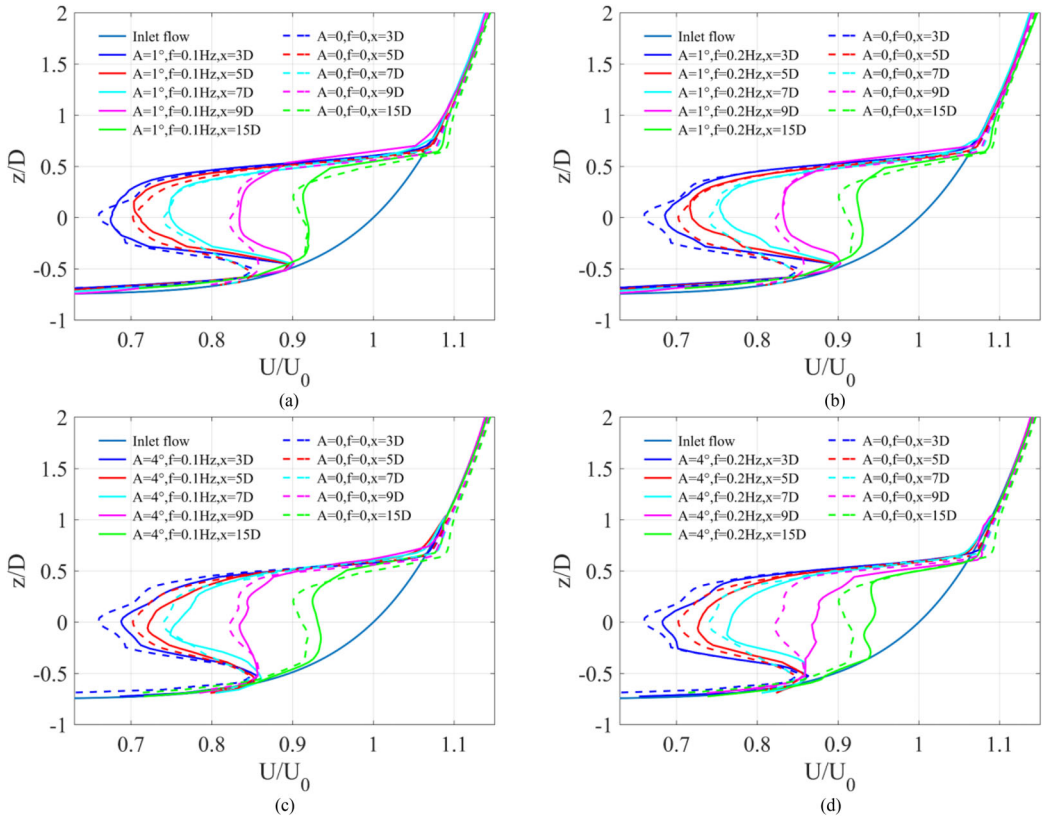

FIGURE 12 Comparison of the vertical mean velocity distribution curve of wake under pitch motion with the results without pitch motion. (a) Case 2, $A = 1$ m, $f = 0.1$ Hz. (b) Case 3, $A = 1$ m, $f = 0.2$ Hz. (c) Case 4, $A = 4$ m, $f = 0.1$ Hz. (d) Case 5, $A = 4$ m, $f = 0.2$ Hz.

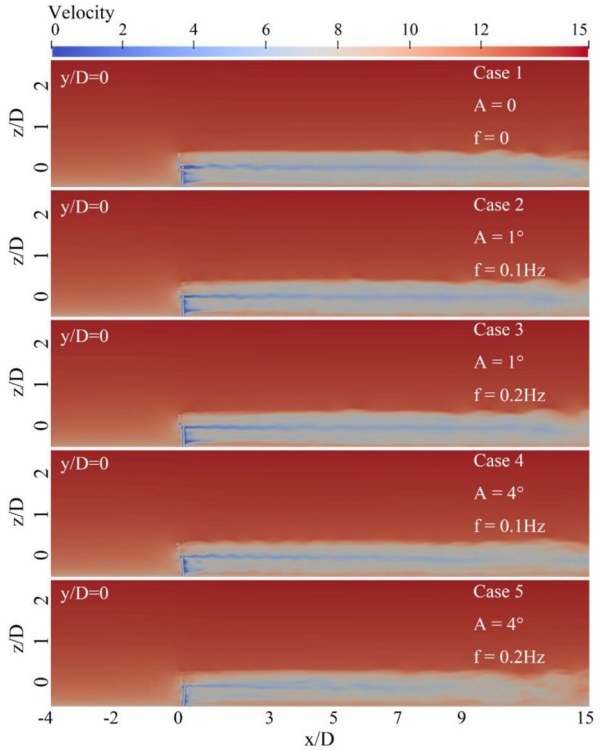

FIGURE 13 The velocity contours of wind turbine wake at x–z plane.

velocity, which aligns with the analytical conclusions drawn from the velocity distribution curve of the wake.

Figure 15 presents the vorticity contour surface with a Q value of 0.02, which visually depicts the flow conditions of the blade tip vortex and the central vortex in the wake flow downstream of the wind turbine. The blade tip vortex and central vortex are subject to the tensile forces of the three-dimensional axial vortex, leading to their rapid decay along the axial direction. By comparing the wake flow conditions across different cases, it can be observed that the tip vortex is more susceptible to being disrupted by the near-field wake perturbations caused by the pitch motion. Additionally, with increasing pitch frequency, the spiral meandering period of the tip vortex and central vortex decreases, while the amplitude of the central vortex meandering increases with the increase in pitch amplitude. However, when the pitch motion has an amplitude of 4° and a frequency of 0.2 Hz, the perturbations caused by the blade become more intense, which results in the intensification of the mixed diffusion of the tip vortex and central vortex. This leads to a reduction in the helical flow spacing of the tip vortex and the destruction of the periodic meandering of the central vortex, resulting in the breaking of the vortex core and an increase in trailing edge vortex shedding. As a result, the recovery of the wake velocity is accelerated.

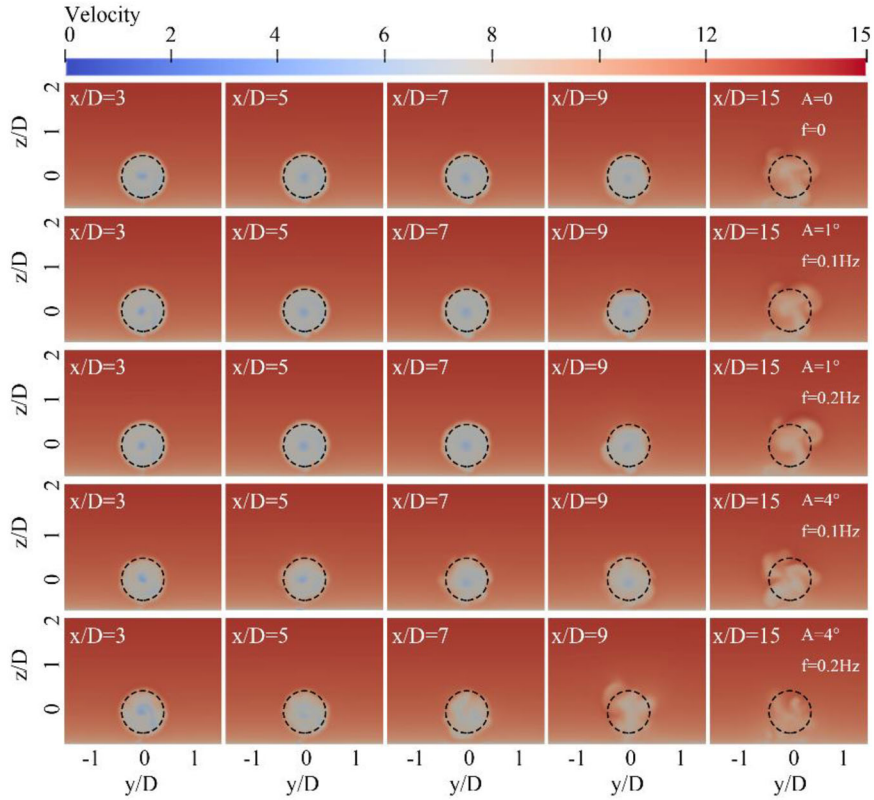

FIGURE 14 The velocity contours of wind turbine wake at y–z plane.

4 | CONCLUSIONS

In this study, the NREL 5MW wind turbine under pitch motion was simulated using the CFD numerical model based on the OpenFOAM, utilizing the overlapping mesh and the numerical simulation method. The results of the simulation provided insight into the aerodynamic power and the wake characteristics of FOWT under pitch motion. The main conclusions of this study are as follows:

1. The results demonstrate the influence of pitch motion on the power and the dynamic changes in the wake characteristics of the wind turbine. The results revealed that the average instantaneous power of the wind turbine increases with the increase in the frequency and amplitude of the pitch motion, leading to larger peaks and smaller valleys in the power output. However, it should be noted that the blade flexibility was not considered in the model, leading to more drastic changes in the blade attack angle and, as a result, greater power fluctuations in the simulations compared to real-life conditions.
2. In comparing the wind velocity distribution curves of the wake under normal conditions to those calculated using the actuator line method model, it is evident that the results of the latter model are deficient in accurately depicting the wind velocity deficit and the extent of the wake influence range in the wake region. Specifically, the calculated wake velocity is exaggerated and the rate of wake velocity recovery, as well as the expansion angle of the wake, are overestimated. This is due to the neglect of the actuator line method of the asymmetric distribution of the wake wind velocity, which is a result of the rotation of the impeller, also neglects the asymmetric distribution of wake wind velocity, which is caused by the rotation of the impeller.
3. The presence of pitch motion in FOWTs results in a perturbation of the surrounding flow field, which leads to an increase in the mixing diffusion speed of the wake and a faster wake recovery rate. When the amplitude of the pitch motion is small, the wind speed recovery of the near wake is slightly affected, while the far wake is not significantly affected. When the amplitude is large, the pitch motion accelerates the wind speed recovery in all wake regions, resulting in more significant diffusion phenomena. This increase in wake recovery rate is observed to be proportional to the frequency and amplitude of the pitch motion. The simulation results show that at a distance of x = 15D downstream from the wind turbine, all cases have essentially recovered to the incoming flow level.

As mentioned above, the effects of pitch motion on FOWTs were investigated under specific operating conditions, and it was found that the influence on the wake and power output increased as the pitch strength increased. The study successfully demonstrated the impact of pitch motion on FOWTs. However, it is important to note that this research only simulated the pitch motion in a 6-DOF motion of FOWTs, and did not take into account the additional impact of 6-DOF motion coupling and the potential effects of flexible blades. Further research is required to fully understand the effects of these factors in future studies.

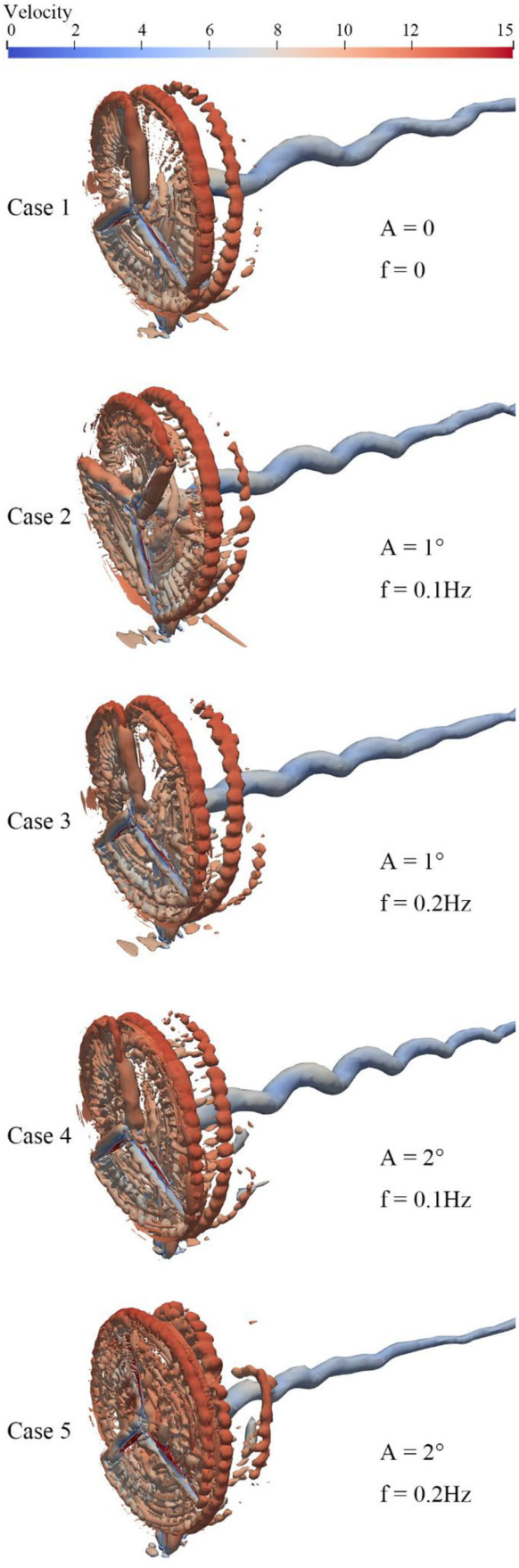

FIGURE 15 3D visualization of the vorticity contour surface of wake.

AUTHOR CONTRIBUTIONS

Rundong Tang: Investigation, Writing - original draft. Renjing Cao: Supervision, Formal analysis, Writing - original draft.

ACKNOWLEDGEMENTS

The Key Program of Marine Economy Development, Department of Natural Resource of Guangdong Province, YZRZH[2022]25 and the support from the Centers for Mechanical Engineering Education and Research at MIT and SUSTech (MechERE Centers at MIT and SUSTech)

CONFLICT OF INTEREST STATEMENT

The authors declare no conflict of interest

DATA AVAILABILITY STATEMENT

Data available on request from the authors.

ORCID

Rundong Tang https://orcid.org/0000-0001-7658-8013

REFERENCES

1. Council, G.W.E.: Global Wind Report 2021 (2021)
2. Heronemus, W.E.: Pollution-Free Energy from the Offshore Winds. Marine Technology Society, pp. 11–13. Washington DC, USA (1972)
3. Henderson, A.R.L.R.: Potential for floating offshore wind energy in Japanese waters. In: Proceedings of The Twelfth International Offshore and Polar Engineering Conference, Kitakyushu, Japan (2002)
4. Duan, L., Li, Y.: Progress of recent research and development in floating offshore wind turbines. SCIENTIA SINICA Physica Mechanica Astronomica 46(12) (2016). https://doi.org/10.1360/sspma2016-00276
5. Thomas Messmer, C.B., Peinke, J., Hölling, M.: A six degree-of-freedom set-up for wind tunnel testing of floating wind turbines. J. Phys. Conf. Ser. 2265(4), 042015 (2022). https://doi.org/10.1088/1742-6596/2265/4/042015
6. Jonkman, J.M.: Dynamics of offshore floating wind turbines—model development and verification. Wind Energy 12, 459–492 (2009)
7. Cordle, A., Jonkman, J.: State of the art in floating wind turbine design tools. In: Presented at the 21st International Offshore and Polar Engineering Conference, vol. 19–24 June 2011, Maui, Hawaii (2011)
8. Nianxin Ren, Y.L., Ou, J.: The motion performance of two offshore wind turbine floating platforms with combined tension leg-mooring line system. In: Proceedings of the Ninth (2010) ISOPE Pacific/Asia Offshore Mechanics Symposium, Korea, vol. 2010, pp. 80–86 (2010)
9. Wei, K., Arwade, S.R., Myers, A.T.: Incremental wind-wave analysis of the structural capacity of offshore wind turbine support structures under extreme loading. Eng. Struct. 79, 58–69 (2014). https://doi.org/10.1016/j.engstruct.2014.08.010
10. Zambrano, C.T.M., Kiceniuk, T., et al.: Dynamic modeling of deepwater offshore wind turbine structures in Gulf of Mexico storm conditions. In: Proceedings of 25th International Conference on Offshore Mechanics and Arctic Engineering, Hamburg, Germany, pp. 1–6 (2006)
11. Micallef, D., Sant, T.: Loading effects on floating offshore horizontal axis wind turbines in surge motion. Renew. Energy 83, 737–748 (2015). https://doi.org/10.1016/j.renene.2015.05.016
12. Tran, T.-T., Kim, D.-H.: The platform pitching motion of floating offshore wind turbine: A preliminary unsteady aerodynamic analysis. J. Wind Eng. Ind. Aerodyn. 142, 65–81 (2015). https://doi.org/10.1016/j.jweia.2015.03.009
13. Lei, W., et al.: Dynamic simulation analysis of floating wind ‘turbine. J. Cent. South Univ. 43(04), 1309–1314 (2012)
14. <number>[14]</numberChen, >W.X., Guo, Y., Kang, S.: Numerical analysis of unsteady aerodynamic performance of floating offshore wind turbine under platform surge and pitch motions. Renew. Energy 163, 1849–1870 (2021). https://doi.org/10.1016/j.renene.2020.10.096

15. Stoelinga, M.S., Poulos, G.S., Crescenti, J.: Estimating long-range external wake losses in energy yield and operational performance assessments using the WRF wind farm parameterization, ArcVera Renewables, 1-19 (2022)
16. Hanson, T.D., Nielsen, F.G., Skaare, B.: Integrated dynamic analysis of floating offshore wind turbines. In: 25th International Conference on Offshore Mechanics and Arctic Engineering. Hamburg, Germany (2006). doi: OMAE 2006–92291:1-9
17. Hand, M.M., Simms, D.A., Fingersh, L.J., Jager, D.W., Cotrell, J.R., Schreck, S.,Larwood, S.M.: Unsteady aerodynamics experiment phase VI: Wind tunnel test configurations and available data campaigns. NREL/TP-500-29955 (2001). https://doi.org/10.2172/15000240
18. Murfet, T., Abdussamie, N.: Loads and response of a tension leg platform wind turbine with non-rotating blades: An experimental study. J. Mar. Sci. Eng. 7(3), 56 (2019). https://doi.org/10.3390/jmse7030056
19. Wang, X., Guo, P., Huang, X.: A review of wind power forecasting models. Energy Procedia 12, 770–778 (2011). https://doi.org/10.1016/j.egypro.2011.10.103
20. Jonkman, J.S.B., Musial, W., Scott, G.: Definition of a 5-MW reference wind turbine for offshore system development. In: Technical Report NREL/TP-500-38060. National Renewable Energy Lab (NREL), Golden, CO (2009)
21. Sezer-Uzol, N., Uzol, O.: Effect of steady and transient wind shear on the wake structure and performance of a horizontal axis wind turbine rotor. Wind Energy 16, 1–17 (2009)
22. Ziwen, C.: Investigations on Unsteady Aerodynamic Characteristics of Floating Offshore Wind Turbine. North China Electric Power University (Beijing) (2021)
23. Jonkman, J.: NREL OffshrBsline5MW (2006)
24. Liu, L.-q., Guo, Y., Zhao, H., Tang, Y.-g.: Motions of a 5 MW floating VAWT evaluated by numerical simulations and model tests. Ocean Eng. 144, 21–34 (2017)
25. Charabi, Y., Abdul-Wahab, S.: Wind turbine performance analysis for energy cost minimization. Renew. Wind Water Solar 7(1), 5 (2020). https://doi.org/10.1186/s40807-020-00062-7
26. Qiang, L., Dynamic Response and Aerodynamic Characteristics of Floating Wind Turbine. University of Chinese Academy of Sciences (2014)
27. Sharpe, D., Burton, T., Jenkins, N., Bossanyi, E.: Wind Energy Handbook. Wiley, New York (2013)
28. Li, Z., Pu, O., Pan, Y., Huang, B., Zhao, Z., Wu, H.: A study on measuring wind turbine wake based on UAV anemometry system. Sustain. Energy Technol. Assess. 53, 102537 (2022). https://doi.org/10.1016/j.seta.2022.102537
29. Sun, H., Yang, H.: Study on an innovative three-dimensional wind turbine wake model. Appl. Energy 226, 483–493 (2018). https://doi.org/10.1016/j.apenergy.2018.06.027

How to cite this article: Tang, R., Cao, R.: Numerical investigation on wake characteristics of floating offshore wind turbine under pitch motion. IET Renew. Power Gener. 1–14 (2023).
https://doi.org/10.1049/rpg2.12741